PCCP

Accepted Manuscript

ROYAL SOCIETY OF CHEMISTRY

www.rsc.org/pccp

Dynamics of the $O(^3P)$ + CH_4 hydrogen abstraction reaction at hyperthermal collision energies

E. Gonzalez-Lavado, C. Rangel, and J. Espinosa-Garcia*
Departamento de Química Física
Universidad de Extremadura, 06071 Badajoz (Spain)
* Corresponding author: joaquin@unex.es

Abstract

Motivated by recent experiments on the title reaction at the high collision energy of 64 kcal mol^{-1} reported by Minton et al., a detailed dynamics study was carried out using quasi-classical trajectory (QCT) calculations based on an analytical potential energy surface recently developed by our group, PES-2014. Our results reproduce the experimental evidence: most of the available energy appears as translational energy (80±10%) and scattering distribution is forward, suggesting a stripping mechanism associated with high impact parameters**.** Of special interest is the triple (angle-velocity) differential cross section (combination of translational and scattering distributions) which shows the same structure associated with the products. Agreement with the experiments lends confidence to the new PES-2014 surface; this is encouraging, furthermore, because its fitting was made with thermal behaviour in mind, and higher energy areas were neither sampled nor weighted sufficiently.

TOC Graphics

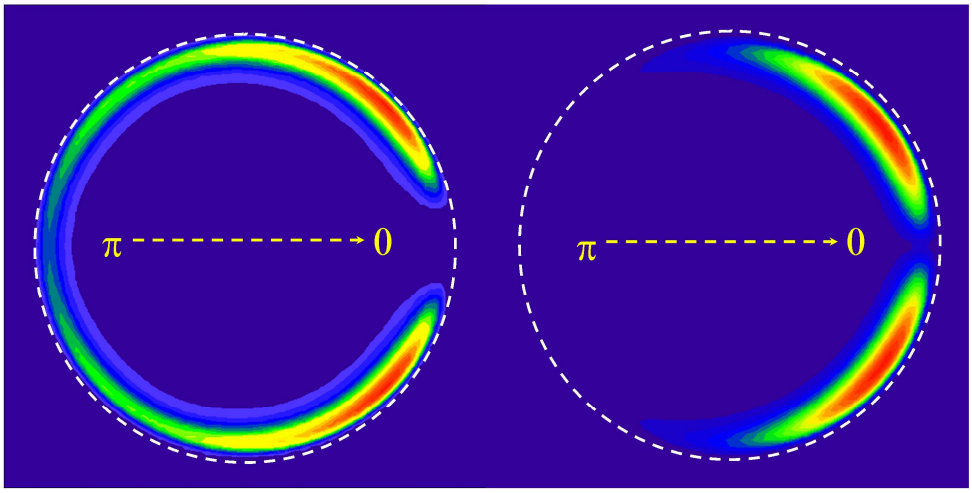

Theoretical results

QCT/PES-2014

Experimental results

Minton and co-workers

Legend: QCT calculations on a full-dimensional analytical potential energy surface (PES-2014) reproduce the experimental dynamics at 64.0 kcal mol^{-1} for the $O(^3P)$ + CH_4 reaction.

I. Introduction

Recently Minton et al.[1] reported experimental studies on the title reaction using two crossed-molecular-beams techniques at hyperthermal collision energies (64 kcal mol^{-1}). They found that the dynamics of the reaction of the O(^{3}P) atom with CH_4 shows forward-scattered distributions associated with a direct abstraction mechanism at large impact parameters.

The O(^{3}P) + CH_4 $\rightarrow$ OH + CH_3 reaction is an interesting system from the experimental point of view, because it is of substantial importance in the chemistry of hydrocarbon combustion (high temperatures); and given that ground-state oxygen atoms are the most abundant species in low Earth orbit (LEO, ≈200-700 Km altitude)[2] this reaction has been used to understand the erosion mechanisms of polymeric materials in the hyperthermal conditions of the LEO.

The dynamics of this reaction (nascent vibrational distributions of the CH_3 product, nascent rotational distributions of the OH product, excitation function and differential cross section) has been widely studied experimentally with different techniques,[3-8] and due to its great experimental interest theoretically, it has also received much attention using different approaches: semiempirical direct dynamics,[9,10] reduced-dimensional quantum molecular (QM) dynamics[11-14] and quasi- classical trajectory (QCT) calculations.[15-19] In addition, a full-dimensional multiconfigurational time-independent Hartree (MCTDH) calculation of the thermal constant was reported.[20] However, most of these studies have been concerned with low collision energies (in the range 8-25 kcal mol^{-1}), and very few at higher energies.[1,9,16] So, while at low collision energies the scattering distribution is backward, associated to a rebound mechanism and low impact parameters, at high collision energies the scattering distribution is forward, associated to a stripping mechanism and high impact parameters.

Theoretically, the accuracy of the dynamics description of a chemical reaction depends mainly on two factors: the dynamics method used, and the potential energy surface (PES) available. In the case of polyatomic systems, QCT calculations have traditionally been the method of choice to study reaction dynamics. Knowledge of the PES plays a crucial role in the study of the dynamics. For the title reaction, great efforts have been made in the construction of its potential energy surface,[16,18,21-23] notably the full-dimensional ab initio PES reported by Czakó and Bowman (CB) in 2012[23] based on a permutationally invariant fit of accurate energy points obtained by an efficient

composite method, and the recent full-dimensional analytical PES developed in our lab,[18] (PES-2014) based exclusively on high-level ab initio calculations. Both surfaces show similar topology, with intermediate complexes in the entrance and exit channels, endothermicity of 5.8 kcal mol^{-1} and barrier height of 14.6 and 14.1 kcal mol^{-1}, respectively, reproducing very high-level calculations,[21] 14.1 kcal mol^{-1}, although the CB surface overestimates this value.

Based on the PES-2014 surface, we performed an exhaustive dynamics study[18] at low collision energies, 8-20 kcal mol^{-1}, reproducing the experimental evidence: the excitation function increased with energy (concave-up), the OH rotovibrational distribution was cold, and the scattering distribution was backward, associated to a rebound mechanism. These results lend confidence to the accuracy of the surface.

In addition to the hydrogen abstraction reaction, at hyperthermal collision energies theoretical and experimental studies[9,24] have reported another pathway, the oxygen-atom addition and subsequent hydrogen-atom elimination yielding H+OCH_3 with a relative yield of 30±10%, its importance increased with the collision energy (above 45 kcal mol^{-1}). However, in the present paper we focus attention on the hydrogen abstraction reaction for a direct comparison with the recent cross beam experiment.[1]

In order to shed more light on the dynamics of the title reaction and the suggested mechanisms and motivated by the recent experimental study[1] at hyperthermal conditions, in the present study we performed QCT calculations on the recent analytical PES-2014 at higher collision energies, 64 kcal mol^{-1}. The article is structured as follows: in Section 2, a brief description of the PES is presented; in Section 3, we briefly outline some computational details of the dynamics calculations; the QCT results are presented in Section 4 and compared with the available experimental data; finally, Section 5 contains the conclusions.

II. Potential energy surface

A complete description of PES-2014 has been given in an earlier paper,[18] and so will not be repeated here. In brief, the functional form is given by

$$V = V_{\text{stretch}} + V_{\text{harm}} + V_{\text{op}} + V_{vdw} \quad (1)$$

where V_{stretch} consists of four LEP-type (London–Eyring–Polanyi) stretching terms, V_{harm} represents the valence bending terms for each bond angle in methane, V_{op}

denotes quadratic-quartic terms whose aim is to correctly describe the out-of-plane motion of methyl, and V_{vdw} is a van der Waals term to describe the intermediate complexes in the entrance and exit channels. In addition a series of switching functions are included to allow the smooth change from pyramidal CH_4 to planar CH_3 product in the hydrogen abstraction reaction. This depends on 41 adjustable parameters, which are fitted to very high level ab initio calculations, CCSD(T) = FULL/aug-cc-pVQZ. The surface presents a barrier height of 14.1 kcal mol^{-1} and a reaction energy of 5.8 kcal mol^{-1}, reproducing benchmark calculations.[23] In addition, it presents intermediate complexes in the entrance and exit channels. This PES was designed to describe exclusively the hydrogen abstraction reaction and was fitted to ab initio calculations in the range of low energies, up to 20 kcal mol^{-1}. Therefore, the results obtained in the present study at 64 kcal mol^{-1} will have a predictive character and will show the consistency of the functional form. For the sake of clarity, Fig. 1 plots schematically the variations in potential energy along the hydrogen abstraction reaction path for PES-2014, together with other theoretical values for comparison.

III. QCT computational details

a) Initial conditions. Based on the PES-2014 surface, QCT calculations were performed using the VENUS96 code.[25] The integration step was 0.01 fs, with an initial separation between the O atom and the methane centre of mass of 10.0 Å. The trajectories were finished when the C-O distance was greater than 11.0 Å. For a direct comparison with the experiment, collision energy is fixed at 64 kcal mol^{-1}. Vibrational energy corresponds to the CH_4 in its ground vibrational state and rotational energies were obtained by thermal sampling at 298 K from a Boltzmann distribution. The maximum value of the impact parameter, b_{max}, is 2.4 Å, determined by calculating batches of 10 000 trajectories at fixed values of the impact parameter, b, the value of b being systematically increased until no reactive trajectories were obtained.

Then 1.000.000 trajectories were calculated with the impact parameter, b, sampled from $b = b_{max}\, R^{1/2}$, where R is a random number in the interval [0, 1].

b) Final conditions. It is well known that one of the difficulties with quasi-classical simulations relates to the question of how to handle the zero-point energy (ZPE) problem. In our previous paper[18] five different alternatives were tested to correct this issue: i) all trajectories are included in the analysis of the results without ZPE

constraint; ii) only those trajectories that lead to both products having a vibrational energy above their ZPEs (DZPE approach) are included, and iii) only the trajectories that lead to the OH product with a vibrational energy above its ZPE are included. Additionally, and in contrast to the previously analyzed histogram binning (HB) approaches in which all trajectories contribute equally to dynamics with weight unity, in the Gaussian binning procedure trajectories are assigned Gaussian statistical weights in such a way that the closer the final vibrational actions to integer values [iv) GB approach][26] or the closer the final total vibrational energy rather than vibrational actions [v) 1GB approach][27] the larger the weights. In the previous paper we found that in general the best agreement with experiment was obtained with the DZPE approach, while the GB and 1GB approaches did not improve this agreement. Therefore, this will be the approach used in the present work.

Finally, the angular scattering distribution of the OH product with respect to the incident O atom was obtained as the differential cross section, DCS, which was fitted by the Legendre moment method.[28]

IV. Results and discussion

IV.1. Product energy partitioning. Table 1 lists the QCT average product fraction of energy in translation, f_{trans}, and in vibration and rotation of CH_3 and OH, $f_{vib}(CH_3)$, $f_{rot}(CH_3)$, $f_{vib}(OH)$, $f_{rot}(OH)$, at 64 kcal mol^{-1}, together with the theoretical values at 15.0 kcal mol^{-1} for comparison. In both collision energies (low and high) the available energy ends up mainly in translational energy, 58±16 and 80±10%, respectively. This result is consistent with the propensity of the heavy-light-heavy mass combination (kinematic constraint) where the excess of translational energy of the reactants is converted predominantly into translational energy of the products. Obviously, when the collision energy increases, the internal energies of the products diminishes from 20 and 22% to 8 and 12%, respectively, for the CH_3 and OH products. The collinear character of the transition state explains the low rotational excitation of the products (≤ 5%). These results are related to the topology of the surface, which has a clear influence on product energy partitioning.

In sum, at 64 kcal mol^{-1} the QCT results show that 80±10% of the available energy goes to translation, thus reproducing the experiment.[1] This result is consistent with the large available energy at hyperthermal collision energy (endothermicity of

only 2.1 kcal mol^{-1}) and a direct hydrogen abstraction/stripping mechanism, where the influence of the intermediate complexes in the entrance and exit channels is negligible.

IV.2. OH product vibrational and rotational distributions. In a previous paper[18] at 15 kcal mol^{-1}, we found that the OH product is practically in its vibrational ground-state, OH(v=0), while the OH rotational distribution is cold, peaking at j=3, reproducing Sweeney et al.'s experiments.[29] This cold rotational distribution was explained based on the C-H'-O collinear attack, as previously noted.

At the higher collision energy studied in the present paper, 64 kcal mol^{-1}, larger vibrational and rotational excitations are expected due to the larger available energy, although no experimental data are available for comparison. Thus, at this energy we find 30% in OH(v=1). Figure 2 plots the OH product rotational distributions for the v=0 and v=1 vibrational states. One observes first that there is a normal negative correlation of product vibrational and rotational excitation, that is, when the vibrational state is excited, v=1, the rotational excitation is lower. So, the rotational population peaks at j=7 and 6 for v=0 and v=1, respectively. This result agrees with universal behaviour for direct bimolecular reactions. Second, the rotational distribution is hotter than at lower energy, 15 kcalmol^{-1}, and extends to high values of j, j=20. However, it is well known that the QCT calculations give rotational distributions hotter and broader than experiments and quantum-mechanical methods.[30-36] Let us consider further this drawback of the QCT methods. Thus, using the harmonic approximation the first excited vibrational state OH(v = 1) is 10.8 kcal mol^{-1} (ω = 3791 cm^{-1}) above the ground state. The QCT results show that the OH rotational population is non-negligible up to j = 20. With a rotational constant B = 18.91 cm^{-1}, this implies an energy (assuming the rigid rotor model) of 22.7 kcal mol^{-1}, which is higher than the first vibrational state energy. In other words, the maximum value of j allowed in the vibrational ground-state is j = 14, i.e., six units less than that obtained in the QCT calculations. This behaviour therefore seems to be an artefact of the QCT methods.

IV.3. Product translational energy distribution. QCT product translational energy distribution is plotted in Figure 3 at collision energy of 64 kcal mol^{-1}, together with the experimental data[1] for comparison. In this experiment the authors[1] noted that the use of a laser to probe the CH_3 product greatly reduced the effective velocity spread of the O-atom beam, as the products being detected must be formed no later than the

moment the probe laser irradiated the products. Theoretically, mimicking these experimental conditions is a rather complicated task because the translational energy is not unique. Therefore, this effect is not included in the QCT calculations, although in accordance with the experiment we expect this effect to be minor.

The QCT results reproduce the experiment, with a fine peak at 55±6 kcal mol^{-1}. This agreement shows that the DZPE criterion to correct the ZPE problem is adequate to describe the present reaction. To analyze the ZPE problem, we also analyzed this property using all reactive trajectories, i.e., without ZPE constraint. We found a similar translational energy distribution (and so we will not represent it here), with the peak slightly shifted, 60±6 kcal mol^{-1}, and therefore with a poorer agreement with the experiment. Consequently, given the small differences, we conclude that the ZPE problem does not significantly affect this property.

IV.4. Product angular distribution. This dynamics property is undoubtedly one of the most sensitive dynamics features with which to test the quality of the potential energy surface. The angular scattering distribution of the OH product with respect to the incident O atom (obtained as the differential cross section, DCS, which is fitted by the Legendre moment method) is plotted in Fig. 4 for the PES-2014 surface. This Figure also includes experimental data[1] for comparison. It was found that the scattering is forward, suggesting a stripping mechanism associated with high impact parameters, thus reproducing the experimental evidence and other theoretical results,[16] although our QCT results present a larger tail at higher scattering angles. So, while the experimental results finish about 120º, our QCT results extend to 180º. This same behaviour was found by Martinez et al.[16] also using QCT calculations but a different PES, which seems to suggest that the differences are associated to the QCT limitations because of its classical nature. As in the previous point on translational energy distribution, we also analyzed the ZPE problem in this property. Considering all reactive trajectories we found a similar behaviour to when the DZPE constraint was considered (Figure 4), and so the influence of the ZPE problem in this property is negligible. Note that in the experiment the OH vibrational states (v=0,1) analyzed in Section IV.2 were not differentiated. The present QCT results permit differentiation of these states. We find similar forward behaviour for both states, with maximum at 45º and 40º, respectively.

In an earlier paper[18] we analyzed dynamics at lower energies (8-20 kcal mol^{-1}) and found that the scattering distribution was backward, evolving to sideways-backward when collision energy increased in this range. Therefore, considering the results from the present work (wider energy range 8-64 kcal mol^{-1}), in this direct hydrogen abstraction reaction the influence of the intermediate complexes in the entrance and exit channels is negligible, and the scattering distribution evolves from backward to forward, i.e., a change of mechanism of reaction is observed, from a rebound to a stripping mechanism (Figure 5). This behaviour is due to the strong correlation between the angular distribution and the impact parameter (Figure 6). In fact, high values of b lead, mainly, to scattering angles in the 0−40° range, while for lower b values the scattering angles are, essentially, in the 140−180° range, i.e., within the forward and backward hemispheres respectively.

To shed more light on the dynamics of the title reaction, the surface plot representing the doubly differential cross section, $d^2\sigma/[d\omega.d\cos(\vartheta)]$, in centre-of-mass polar coordinates (ω, θ) are shown in Fig. 7 at a collision energy of 64 kcal mol^{-1}. The QCT results show forward scattering, in agreement with the experimental evidence.[1] The largest difference is the more backward character of the theoretical calculations which is probably due to limitations of the theoretical approaches (surface and QCT calculations).

V. Conclusions

In general, when comparing theoretical and experimental dynamics results, many factors are involved. First, of course, there is the quality and accuracy of the experimental data. And second, theoretically the dynamics method used (quasi-classical or quantum mechanical) and the accuracy of the potential energy surface must be taken into account. Therefore, in a theory/experiment comparison, both the dynamics method and the PES are being tested.

In our comparison with recent delicate experiments reported by Minton et al., we showed that, despite their classical nature, QCT calculations may provide a state-resolved picture that is comparable with the experiment when the calculations are analyzed with a quantum spirit. The theory/experiment agreement at high collision energies is encouraging, because the PES-2014 was fitted to reproduce ab initio calculations of low energy, i.e., reaction path and reaction valley. Therefore, these

results at high energies lend confidence to the accuracy of the PES-2014, which "captures" the essence of the dynamics reaction.

Since it is still a very challenging—if not impossible—task to obtain detailed information such as differential cross sections from a full-dimensional quantum dynamics calculation of a reaction involving more than three-four atoms, reduced dimensionality quantum scattering or quasi-classical trajectory calculations represent the only alternative at present for the analysis of polyatomic systems.

ACKNOWLEDGMENTS

This work was partially supported by Gobierno de Extremadura, Spain (Project No. IB10001). We thank Prof. Timothy Minton the experimental data to plot Fig. 7.

References

1. J. Zhang, S.A. Lahankar, D.J. Garton, T.K. Minton, W. Zhang, and X. Yang, *J.Phys.Chem. A*, 2011, **115**, 10894.
2. K.S.W. Champion, A.E. Cole, and A.J. Kantor, In *Handbook of Geophysics and the Space EnVironment*; A.S. Jursa, Ed.; Air Force Geophysics Laboratory, Air Force Systems Command, United States Air Force, 1985.
3. T. Suzuki, and E. Hirota, J.Chem.Phys. 1993, **98**, 2387.
4. G.M. Sweeney, A. Watson, and K.G. McKendrick, J.Chem.Phys. 1997, **106**, 9182.
5. F. Ausfelder, H. Kelso, amd K.G. McKendrick, Phys.Chem.Chem.Phys. 2002, **4**, 473.
6. B. Zhang, and K. Liu, J. Phys. Chem. A 2005, **109**, 6791.
7. F. Wang, and K. Liu, Chem. Sci. 2010, **1**, 126.
8. B. Zhang, and K. Liu, Chem. Asian J. 2011, **6**, 3132.
9. D. Troya, R.A. Pascual, and G.C. Schatz, J.Phys.Chem. A 2003, **107**, 10497.
10. D. Troya, and E. García-Molina, J.Phys.Chem. A 2005, **109**, 3015.
11. H-G. Yu, and G. Nyman, J. Chem. Phys. 2000, **112**, 238.
12. J. Palma, and D.C. Clary, J. Chem. Phys. 2000, **112**, 1859.
13. J. Palma, and D.C. Clary, J. Chem. Phys. 2001, **115**, 2188.
14. M. Yang, S-Y. Lee, and D.H. Zhang, J. Chem. Phys. 2007, **126**, 064303.
15. M. González, J. Hernando, J. Millán, and R. Sayós, J. Chem. Phys. 1999, **110**, 7326.
16. R. Martinez, P.A. Enriquez, M.P. Puyuelo, and M. Gonzalez, J. Phys. Chem. A 2012, **116**, 5026.

17. G. Czakó, R. Liu, M. Yang, J.M. Bowman, and H. Guo, J.Phys.Chem. A 2013, **117**, 6409.
18. E. Gonzalez-Lavado, J.C. Corchado, and J. Espinosa-Garcia, J.Chem.Phys. 2014, **140**, 064310.
19. R. Liu, M. Yang, G. Czako, J.M. Bowman, J. Li, and H. Guo, J.Phys.Chem Letters 2012, **3**, 3776.
20. F. Huarte-Larrañaga, and U. Manthe, J.Chem.Phys. 2002, **117**, 4635.
21. J. Espinosa-Garcia, and J.C. García-Bernaldez, Phys. Chem. Chem. Phys. 2000, **2**, 2345.
22. Y. Liu, Y. Gao, H. Zhai, D. Shi, and J. Sun, Int. J. Molecular Science 2009, **10**, 2146.
23. G. Czako, and J.M. Bowman, PNAS 2012, **109**, 7997.
24. D. Troya, G.C. Schatz, D.J. Garton, A.L. Brunsvold, and T.K. Minton, J. Chem. Phys. 2004, **120**, 731.
25. W.L. Hase, R.J. Duchovic, X. Hu, A. Komornicki, K.F. Lim, D.h. Lu, G.H. Peslherbe, K.N. Swamy, S.R. Vande Linde, A.J.C. Varandas, H. Wang, and R.J. Wolf, VENUS96: A General Chemical Dynamics Computer Program, QCPE Bull. 1996, **16,** 43.
26. L. Bonnet, J. Chem. Phys. 2008, **128**, 044109.
27. G. Czakó, and J.M. Bowman, J. Chem. Phys. 2009, **131**, 244302.
28. D.G. Truhlar, and N.C. Blais, J.Chem. Phys. 1977, **67**, 1532.
29. G.M. Sweeney, A. Watson, and K.G. McKendrick, J.Chem.Phys. 1997, **106**, 9172.
30. L. Bañares, F.J. Aoiz, P. Honvault, B. Bussery-Honvault, and J-M. Launay, J. Chem. Phys. 2003**, 118,** 565.
31. D.P. Gerrity, and J.J. Valentini, J. Chem. Phys. 1984, **81**, 1298.
32. D.A.V. Kliner, K.D. Rinnen, and R.N. Zare, Chem. Phys. Lett. 1990, **166**, 107.
33. B.D. Bean, F. Fernandez-Alonso, and R.N. Zare, J. Phys. Chem. A 2001**, 105**, 2228.
34. B.D. Bean, J.D. Ayers, F. Fernandez-Alonso, and R.N. Zare, J. Chem. Phys. 2002**,** **116**, 6634.
35. A.E. Pomerantz, F. Ausfelder, R.N. Zare, S.C. Althorpe, F.J. Aoiz, L. Bañares, F.J. Castillo, J. Chem. Phys. 2004**, 120**, 3244.
36. T. Xie, J.M. Bowman, J.W. Duff, M. Braunstein, and B. Ramachandran, J. Chem. Phys. 2005**, 122**, 014301.

Table 1. Product energy partitioning (percentages) for the $O(^3P) + CH_4$ reaction.

Collision energy	f_{trans}	$f_{vib}(CH_3)$	$f_{rot}(CH_3)$	$f_{vib}(OH)$	$f_{rot}(OH)$
64 kcal mol^{-1}	80±10	6±5	2±2	7±6	5±5
15 kcal mol^{-1}	58±16	15±13	5±4	18±14	4±6

Error bars representing ±1 standard deviation are indicated.

FIGURE CAPTIONS

Figure 1: Schematic profile of the potential energy surface along the reaction path. CCSD(T): CCSD(T)=FULL/aug-cc-pVQZ//CCSD(T)=FC/cc-pVTZ single point level from Ref. 18; PES-2014: using the analytical surface developed in Ref. 18; Benchmark: Accurate relative energies obtained at the all-electron CCSDT(Q)/complete-basis-set quality from Ref. 21.

Figure 2. Rotational populations for OH(v,j) product for the v=0 (blue line) and v=1(red line) vibrational states at collision energy of 64 kcal·mol^{-1}.

Figure 3. Product translational energy distribution (PTD) at a collision energy of 64 kcal·mol^{-1}. Solid line: QCT/PES-2014 calculations. The error bar is 6 kcal mol^{-1} representing ±1 standard deviation. Dotted line: Experimental data from Ref. 1.

Figure 4. OH product angular distribution (with respect to the incident O) for the title reaction at 64 kcal mol^{-1}. Solid line: QCT/PES-2014 results; dotted line: experimental values.[1] Given the large number of trajectories, the error bars are negligible and they have not been represented.

Figure 5. QCT/PES-2014 product angular distribution for the title reaction, in the energy range 8-64 kcal mol^{-1}.

Figure 6. Scattering angle (degrees) as a function of the impact parameter (angstrom).

Figure 7. QCT polar scattering three-dimensional surface plot and contour map of the CM scattering angle-velocity distribution, $P(\omega,\theta)$, for the OH products of the title reaction at 64 kcal mol^{-1}. CM velocity in m.s^{-1}. Left panel: Theoretical results from this work; right panel: Experimental results from Ref. 1.

Figure 1

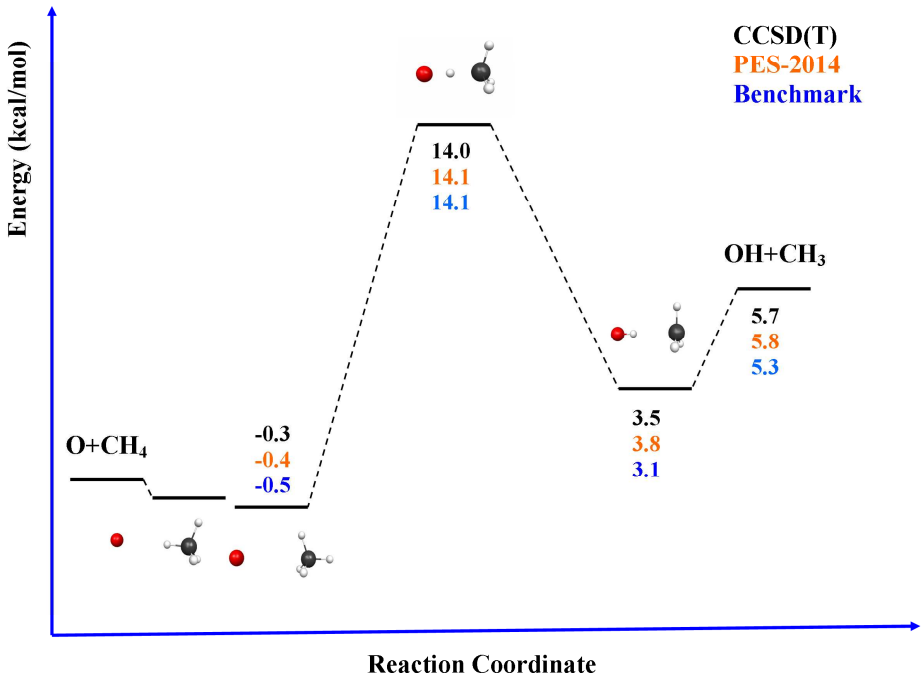

Figure 2

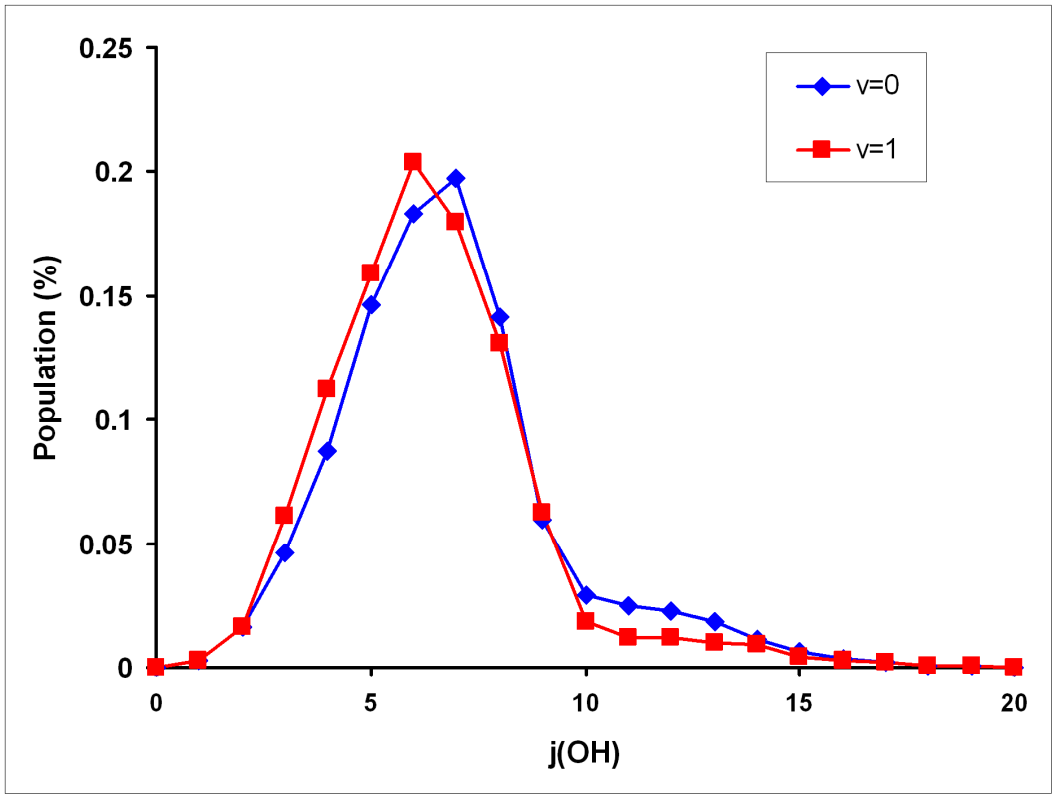

Figure 3

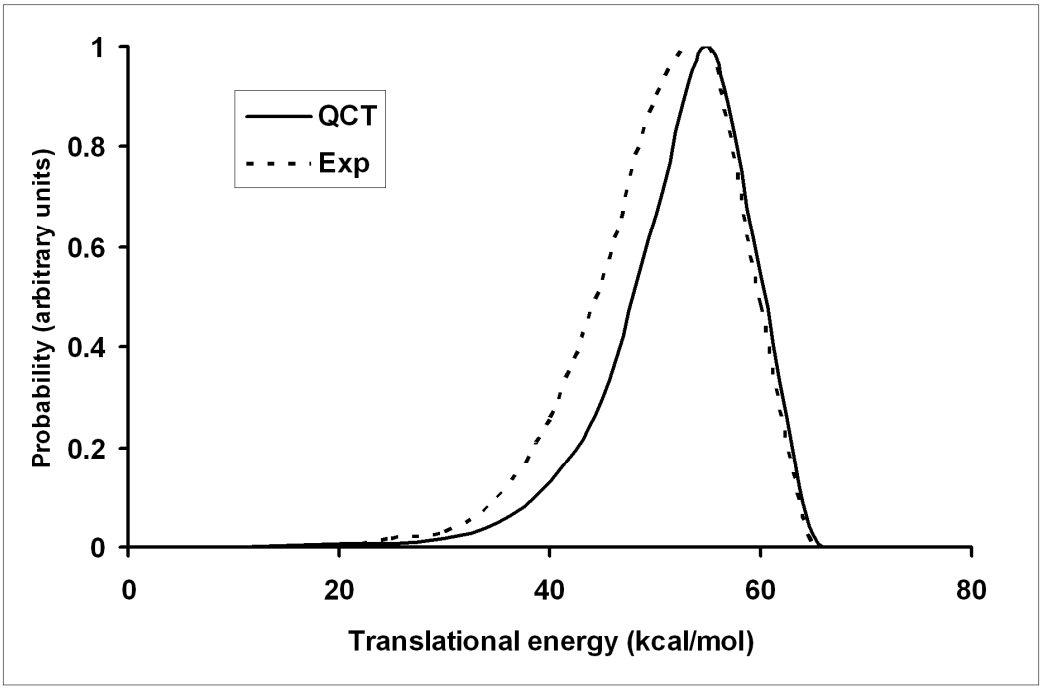

Figure 4

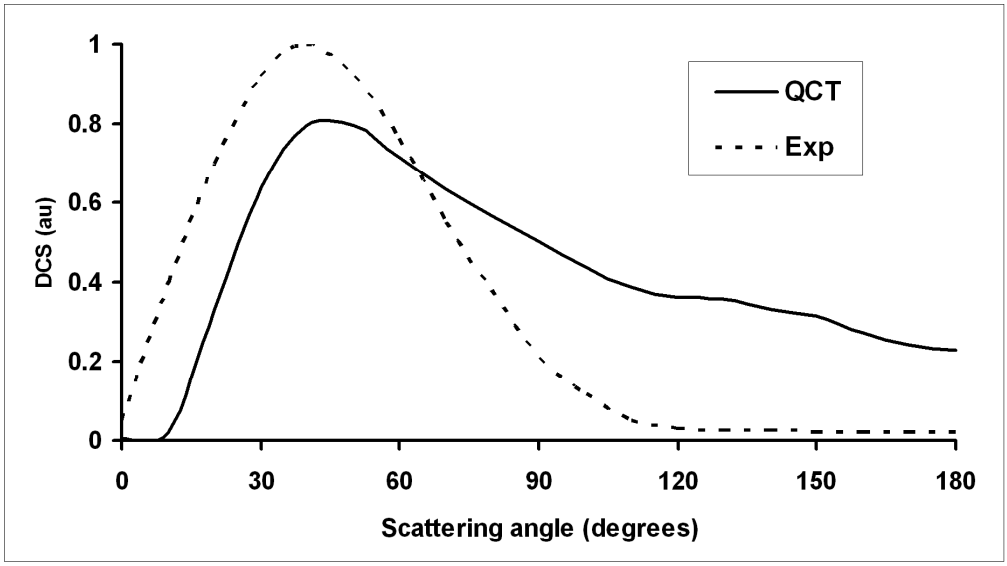

Figure 5

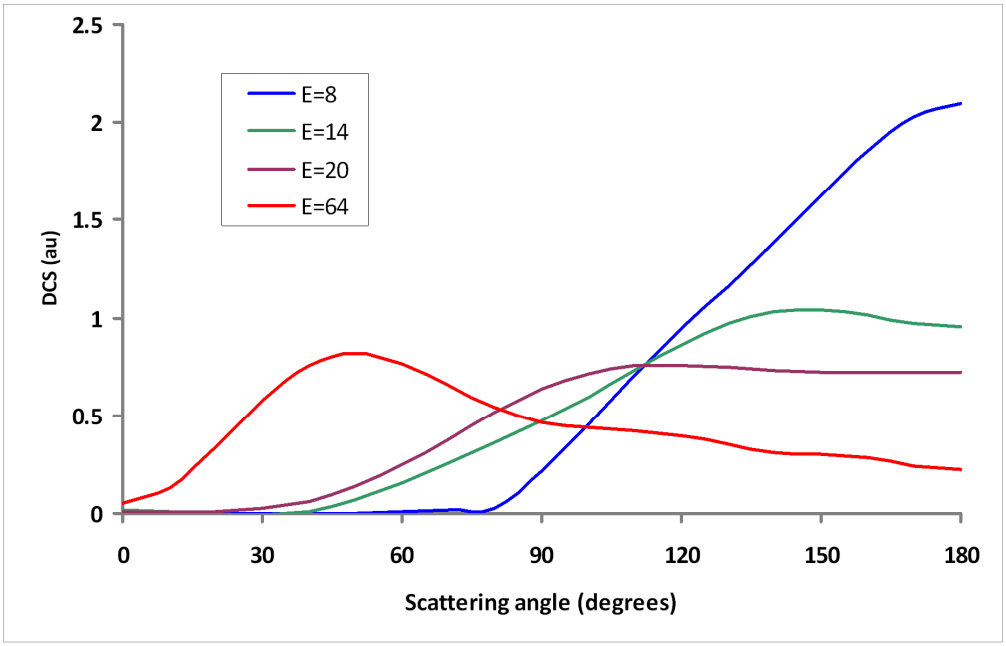

Figure 6

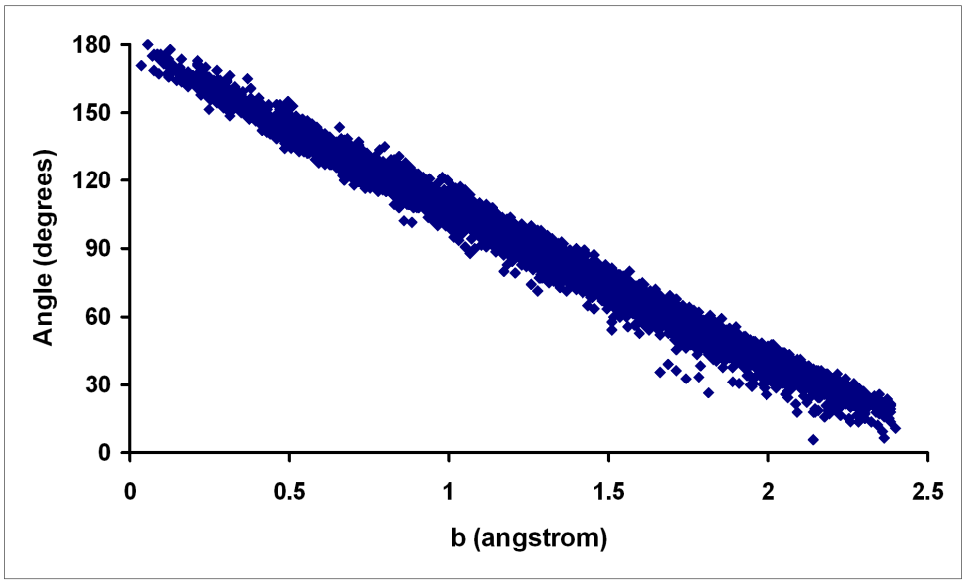

Figure 7